Palladium interaction with CeO_2, Sn–Ce–O and Ga–Ce–O layers

2009 J. Phys.: Condens. Matter 21 055005

(http://iopscience.iop.org/0953-8984/21/5/055005)

J. Phys.: Condens. Matter **21** (2009) 055005 (9pp) doi:10.1088/0953-8984/21/5/055005

Palladium interaction with CeO_2, Sn–Ce–O and Ga–Ce–O layers

T Skála[1], F Šutara[2,3], M Škoda[2], K C Prince[1] and V Matolín[2]

[1] Sincrotrone Trieste, Strada Statale 14, km 163.5, I-34012 Basovizza-Trieste, Italy
[2] Charles University, Faculty of Mathematics and Physics, Department of Surface and Plasma Science, V Holešovičkách 2, CZ-18000 Prague 8, Czech Republic

E-mail: tomas.skala@elettra.trieste.it

Received 22 October 2008, in final form 20 November 2008
Published 16 December 2008
Online at stacks.iop.org/JPhysCM/21/055005

Abstract
Using photoemission, we have studied the interaction of palladium with thin layers of stoichiometric ceria (Ce^{4+} character) and two mixed oxides, Ga–Ce–O and Sn–Ce–O, where cerium in the Ce^{3+} oxidation state is present. Palladium was found to partially reduce the CeO_2 layer by introducing oxygen vacancies most probably in the vicinity of the growing Pd particles. In mixed oxide systems palladium very strongly interacts with both added metals—gallium and tin—leading to a breaking of metal–ceria bonds and the establishment of Pd–Ga(Sn) intermetallic compounds. As a consequence the ceria reoxidizes back to a Ce^{4+} oxidation state.

(Some figures in this article are in colour only in the electronic version)

1. Introduction

Cerium dioxide, or ceria, is an important material for many industrial applications with a variety of excellent properties, for example optical (high refractive index, high transmission, violet and blue emission), mechanical (hardness, stability towards abrasion, high adhesion), and thermal and chemical stability [1]. Due to its catalytic properties it forms a necessary part of three-way catalysts and solid oxide fuel cells.

For catalytic applications, a key feature of ceria is its ability to release a part of its oxygen content and provide it to the catalytic reaction. This property is reversible, so that ceria acts as an oxygen buffer. The oxygen release is accompanied by transformation of cerium from the Ce^{4+} oxidation state to Ce^{3+}. The activation energy for this stoichiometry alteration is relatively low, and under oxidizing conditions the partially reduced ceria can be reoxidized back to a CeO_2 stoichiometry.

The oxygen storage capacity of ceria can be improved by additives, of which one important group is formed by other oxides such as ZrO_2, Al_2O_3 or SnO_2, i.e. materials often used as supports in catalysis. Their interaction with ceria can result not only in a different surface morphology but the oxygen storage capacity can be influenced chemically. Stronger mutual interaction leads, for example, to formation of a mixed oxide that exhibits better catalytic properties than the individual oxides, for example Sn–Ce–O versus SnO_2 and CeO_2 in [2]. In the case of additive metals very strongly interacting with cerium such as tin or gallium, the mixed oxide can be easily prepared by deposition of the metal onto CeO_2. This approach can be used in both real catalysts and well-defined model systems studied to understand elementary processes on the surfaces.

A second important group of additives to cerium oxide systems are transition metals. In catalysis, these metals are usually deposited on various oxide substrates, forming particles of nanometre size, thus providing a large surface area for the catalytic reaction while the total amount of the metal is small, to decrease the cost of the catalyst. On catalytically active substrates the transition metals provide adsorption sites for some of the reactants, resulting in a substantial improvement in the catalytic activity of the system.

One of the most used transition metals in catalysis is palladium. A prototypical reaction is the oxidation of carbon monoxide on a Pd/CeO_2 system where palladium is a typical member of a group of transition metals on whose surfaces CO molecules easily adsorb and ceria can provide oxygen for the reaction [3, 4]. Other important reactions catalyzed by palladium/ceria are methane steam reforming [5] and combustion [6], hydrodechlorination of chlorobenzene [7], methanol and ethanol decomposition [8, 9], and NO_x reduction [10]. An analysis of STM images by

[3] Present address: Physics Department, CINVESTAV-IPN, Avenue IPN 2508, MX-07360 Mexico City, DF, Mexico.

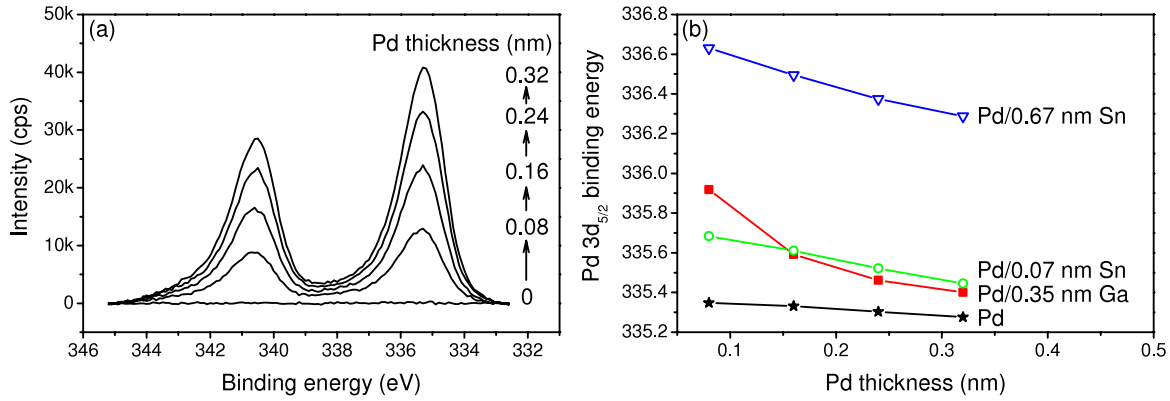

Figure 1. Pd 3d XPS spectra measured after each deposition step of Pd onto the prepared CeO_2 layer (a) and the evolution of the binding energy of the Pd $3d_{5/2}$ peak after each deposition step onto CeO_2 (stars), Ga–Ce–O (squares) and both Sn–Ce–O (circles and triangles) layers (b). Photon energy: 1486.6 eV.

Sennanayake *et al* confirmed that palladium deposited onto a CeO_2 layer at 300 K forms flat islands of several nanometres in diameter [4]. CO adsorbs only molecularly on palladium and the adsorption becomes partially dissociative when Pd islands are activated by partially reduced ceria. This stoichiometry alteration can be induced by the presence of palladium itself since its interaction with ceria may introduce oxygen vacancies and improve slightly the oxygen storage capacity, as confirmed both experimentally [11] and by theoretical calculations [12].

The chemical state of cerium is often determined by analysing the photoelectron spectra of the Ce 3d or 4d core levels. The analysis of these core level spectra is not straightforward since in both stable cerium oxides (cerium dioxide and trioxide), several different 4f configurations in the photoemission final states exist. Fitting procedures performed on these spectra in order to determine quantitatively the ratio of Ce^{3+} and Ce^{4+} species require the consideration of a relatively large number of partially overlapping peaks. Resonant photoemission using tunable synchrotron radiation provides another approach for monitoring the effects of the reversible $Ce^{4+} \leftrightarrow Ce^{3+}$ transition. This method utilizes resonances of the 4f electron lines in the valence band spectra acquired near the Ce 4d $\rightarrow$ 4f photoabsorption region [13]. The constant initial state curves acquired in our previous experiments revealed that at photon energy 115 eV there are no resonances (off-resonance), at 121.4 eV the Ce^{3+} states around the binding energy 1.5 eV resonate, and at 124.8 eV the Ce^{4+} states around binding energy 4 eV also resonate [14]. The net resonance enhancement ratio D can be calculated by dividing these two resonant maxima after subtraction of the off-resonance spectrum. This approach is more sensitive to even fine variations of the cerium chemical state and does not suffer from problems with difficult and therefore sometimes ambiguous fitting procedures performed on the core levels.

Previously we investigated the interaction of metallic gallium [14] and tin [15, 16] layers with CeO_2. These metals caused strong reduction of the stoichiometric ceria surfaces. In the present paper we describe the interaction of palladium with these Ga–Ce–O and Sn–Ce–O mixed oxides. These results are compared with those obtained on the Pd/CeO_2 system without any other metal.

2. Experimental details

The measurements were carried out in an ultra-high vacuum chamber (base pressure below 1×10^{-8} Pa) at the Materials Science Beamline at the Elettra synchrotron light source in Trieste. The sample was a copper disc (∅ 10 mm × 2 mm) supplied by MaTecK with a polished surface oriented to within 0.1° of the (1 1 1) plane, and cleaned *in situ* by cycles of Ar^+ ion sputtering (1000 eV, 15 μA cm^{-2}) and annealing by resistively heated tantalum wires to 723 K. No impurities were detectable by XPS (x-ray photoelectron spectroscopy) and LEED (low energy electron diffraction) showed a sharp (1×1) pattern.

Cerium was evaporated from a molybdenum crucible heated by electron bombardment in 5×10^{-5} Pa of oxygen to deposit a 1.5 nm thick epitaxial layer onto the copper surface at 523 K. The stoichiometric CeO_2(1 1 1) layer was characterized as in our previous work [17]. Onto the prepared CeO_2 layer we deposited the following metals: up to 0.32 nm of palladium in four equidistant steps (using an electron-beam-heated Pd wire); 0.35 nm of gallium (from a resistively heated quartz crucible); lower (0.07 nm) and higher (0.67 nm) amounts of tin (from a pyrolytic graphite crucible heated by electron bombardment). In all cases the temperature of the sample was 300 K.

The interaction of Pd with CeO_2, Ga–Ce–O and Sn–Ce–O layers was studied by XPS using an Al Kα laboratory x-ray source (1486.6 eV) for Cu $2p_{3/2}$, Ce 3d, Pd 3d, Ga $2p_{3/2}$, Sn $3d_{3/2}$, O 1s and C 1s lines, and with monochromatized synchrotron photons (115, 121.4 and 124.8 eV for resonances in the valence band spectra and 115 eV for the Ga 3d and Sn 4d lines). The synchrotron data were normalized to the incident photon flux. The electron emission angle was 20° and 0° with respect to the surface normal for Al Kα and synchrotron-radiation-excited spectra and the total resolution (analyser + photons) was 1 and 0.18 eV, respectively.

3. Results and discussion

3.1. Pd/CeO$_2$ system

XPS spectra of the palladium 3d line after each deposition step are shown in figure 1(a). With increasing amounts of palladium the doublet intensity does not grow linearly. The

Table 1. Voigt fitting parameters of the Ce 3d levels on the Pd/CeO_2 sample. The spin–orbit splitting was set to 18.53 eV. The asymmetry of the Ce^{4+} 3d $u + v$ doublet was modelled by another Voigt doublet shifted by 1.30 eV towards higher binding energies, with Lorentzian width 0.48 eV, Gaussian width 3.20 eV and intensity ratio 0.50 with respect to the $u + v$ one.

	Pd thickness (nm)	0.00	0.08	0.16	0.24	0.32
Ce^{4+}	Binding energy $3d_{5/2}$ (eV)	882.25	882.35	882.40	882.45	882.45
$u + v$	Relative intensity	0.30	0.29	0.28	0.28	0.28
	Lorentzian width (eV)	1.35	1.35	1.35	1.35	1.35
	Gaussian width (eV)	1.03	1.03	1.03	1.03	1.03
	Branching ratio	0.70	0.70	0.70	0.70	0.70
Ce^{4+}	Binding energy $3d_{5/2}$ (eV)	888.80	888.90	888.95	889.00	889.00
$u'' + v''$	Relative intensity	0.38	0.36	0.35	0.34	0.33
	Lorentzian width (eV)	4.01	4.01	4.01	4.01	4.01
	Gaussian width (eV)	2.09	2.09	2.09	2.09	2.09
	Branching ratio	0.61	0.61	0.61	0.61	0.61
Ce^{4+}	Binding energy $3d_{5/2}$ (eV)	898.25	898.35	898.40	898.40	898.45
$u''' + v'''$	Relative intensity	0.31	0.31	0.31	0.30	0.30
	Lorentzian width (eV)	1.60	1.60	1.60	1.60	1.60
	Gaussian width (eV)	1.26	1.26	1.26	1.26	1.26
	Branching ratio	0.71	0.71	0.71	0.71	0.71
Ce^{3+}	Binding energy $3d_{5/2}$ (eV)	—	880.55	880.65	880.65	880.65
$u_0 + v_0$	Relative intensity	0.00	0.01	0.01	0.02	0.02
	Lorentzian width (eV)	—	0.93	0.93	0.93	0.93
	Gaussian width (eV)	—	1.73	1.73	1.73	1.73
	Branching ratio	—	0.56	0.56	0.56	0.56
Ce^{3+}	Binding energy $3d_{5/2}$ (eV)	885.35	885.45	885.55	885.55	885.55
$u' + v'$	Relative intensity	0.01	0.03	0.05	0.06	0.07
	Lorentzian width (eV)	4.47	4.47	4.47	4.47	4.47
	Gaussian width (eV)	0.57	0.57	0.57	0.57	0.57
	Branching ratio	0.56	0.56	0.56	0.56	0.56

binding energy of the Pd $3d_{5/2}$ peak plotted with star symbols in figure 1(b) slowly decreases after each deposition step, from 335.35 eV at 0.08 nm to about 335.25 eV at 0.32 nm. These values are always higher than the binding energy of the Pd $3d_{5/2}$ peak measured under the same conditions on pure metals (335.1 eV on a clean Pd(1 1 1) single crystal and 335.15 eV on a polycrystalline foil). This behaviour is typical for growth of small three-dimensional clusters and is similar to the case of Pd on weakly interacting oxides like alumina [18]. The binding energy is higher for ultra-thin deposits due to the reduction of screening effects and the final-state energy variation. We note that this shift cannot be caused by band bending or charging effects because it is quantitatively different from the shifts of the Ce 3d levels that will be presented later.

The influence of palladium clusters on the ceria layer was studied by measuring the Ce 3d core levels. The spectra before the first and after the fourth deposition step are shown in figure 2. The spectra were fitted using three doublets ($u + v$ asymmetric composed of two summed constrained Voigt profiles and $u'' + v''$, $u''' + v'''$ Voigt ones) representing the Ce^{4+} states and two doublets ($u_0 + v_0$ and $u' + v'$, all Voigt) for the Ce^{3+} states. The details of the peak fitting used in our data evaluation were described in [19] and the fitting parameters are summarized in table 1. In figure 2(a) it can be seen that the contribution of the Ce^{3+} states in the prepared ceria layer was very low, below 1%, indicating good CeO_2 stoichiometry. Upon deposition of palladium the ceria layer was partially reduced, with the Ce^{3+} states' contribution to the Ce 3d spectra reaching 9% after the last deposition step. The complete evolution of the Ce^{3+}/Ce^{4+} ratio is plotted with star symbols in figure 3(a). The interaction of Pd with CeO_2 is relatively weak at 300 K compared to other metals in this study, as we will show later.

Figure 4 shows valence band spectra of the ceria layer with 0.32 nm of Pd measured using synchrotron radiation in the proximity of the Ce 4d → 4f resonance. The evolution of the D ratio, describing the extent of reduction with high sensitivity and low information depth, after each deposition step is plotted in figure 3(b). On the as-prepared CeO_2 layer its value was below 0.03 and in the presence of palladium clusters it slowly increases to 0.51.

3.2. Pd/Ga–Ce–O system

The Ga–Ce–O system was prepared by depositing 0.35 nm of metallic gallium onto a stoichiometric 1.5 nm thick CeO_2 layer at 300 K. As reported in [14], the interaction of Ga with Ce leads to partial reduction of CeO_2 and oxidation of Ga resulting in the formation of mixed gallium–cerium oxide. Ce^{3+}-related features appeared in the Ce 3d spectra and the Ce^{3+}/Ce^{4+} area ratio was 0.61. The fitting parameters are summarized in table 2. At the same time the ratio D of the resonance enhancements of the Ce^{3+} and Ce^{4+} states in the valence band spectra reached the value 2.9. Ga $2p_{3/2}$ spectra contained a single peak at binding energy 1118.35 eV and the Ga 3d spectra a broad feature that we suggested to decompose into two unresolved doublets assigned to oxides, see bottom curves in figures 5(a) and (b), respectively. The parameters of the peak fitting are in tables 3 and 4, respectively. For further details see [14].

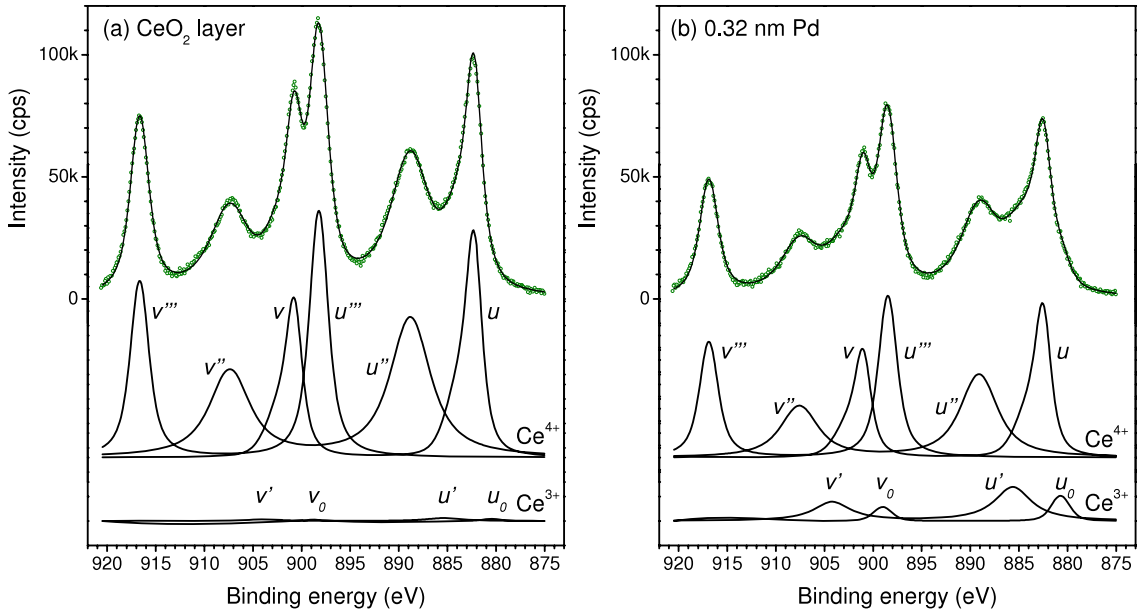

Figure 2. Ce 3d XPS spectra measured on the prepared CeO_2 layer (a) and after the last deposition of Pd (b). The fits of the spectra with Ce^{3+} and Ce^{4+} states are shown in the lower part of the figures. Photon energy: 1486.6 eV.

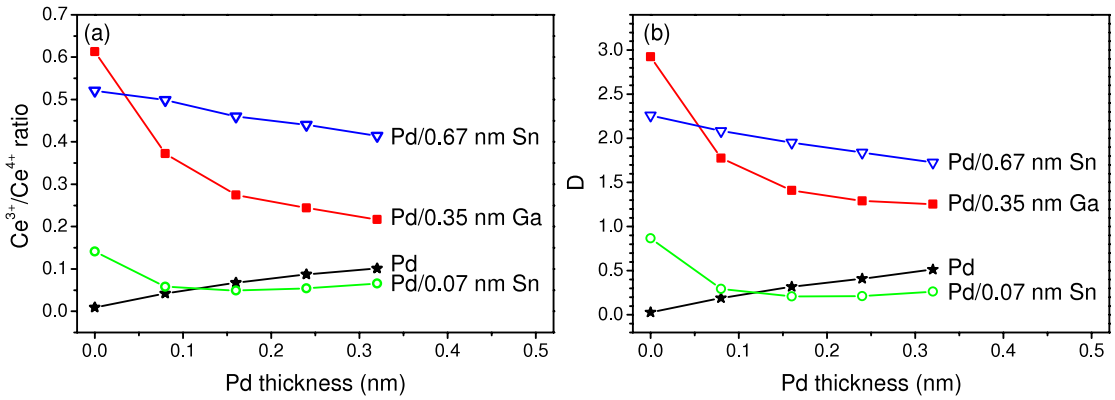

Figure 3. Evolution of the Ce^{3+}/Ce^{4+} 3d XPS intensity ratio (a) and resonance enhancement ratio D (b) upon the deposition of palladium onto CeO_2 (stars), Ga–Ce–O (squares) and two different Sn–Ce–O (circles and triangles) layers.

Table 2. Voigt fitting parameters of the Ce 3d levels on the Pd/Ga–Ce–O sample. The spin–orbit splitting, asymmetry modelling, widths and branching ratios are the same as in table 1.

	Pd thickness (nm)	0.00	0.08	0.16	0.24	0.32
Ce^{4+}	Binding energy $3d_{5/2}$ (eV)	882.55	882.55	882.55	882.50	882.50
$u + v$	Relative intensity	0.26	0.29	0.30	0.30	0.30
Ce^{4+}	Binding energy $3d_{5/2}$ (eV)	889.35	889.35	889.35	889.30	889.20
$u'' + v''$	Relative intensity	0.13	0.17	0.19	0.20	0.21
Ce^{4+}	Binding energy $3d_{5/2}$ (eV)	898.55	898.55	898.50	898.50	898.45
$u''' + v'''$	Relative intensity	0.23	0.27	0.30	0.30	0.31
Ce^{3+}	Binding energy $3d_{5/2}$ (eV)	880.80	880.80	880.75	880.70	880.70
$u_0 + v_0$	Relative intensity	0.12	0.08	0.06	0.06	0.05
Ce^{3+}	Binding energy $3d_{5/2}$ (eV)	885.75	885.75	885.70	885.70	885.70
$u' + v'$	Relative intensity	0.26	0.19	0.15	0.14	0.13

The evolution of the Ce^{3+}/Ce^{4+} ratio calculated from the fitting of the Ce 3d core level spectra and of the ratio D shows an interesting behaviour upon the deposition of palladium onto the mixed oxide surface, opposite to that of the pure ceria layer. Both of these measures of the Ce^{3+} content decrease with increasing thickness of the Pd layer, i.e. the cerium oxide stoichiometry changes back towards the original CeO_2. As expected from our previous study [20]

Table 3. Voigt fitting parameters of the Ga $2p_{3/2}$ line on the Ga–Ce–O sample.

	Pd thickness (nm)	0.00	0.08	0.16	0.24	0.32
Oxide component	Binding energy (eV)	1118.35	1117.80	1117.80	1117.80	1117.80
	Relative intensity	1.00	0.88	0.76	0.70	0.66
	Lorentzian width (eV)	1.18	1.18	1.18	1.18	1.18
	Gaussian width (eV)	1.37	1.37	1.37	1.37	1.37
Intermetallic component	Binding energy (eV)	—	1116.55	1116.55	1116.55	1116.55
	Relative intensity	0.00	0.12	0.24	0.30	0.34
	Lorentzian width (eV)	—	1.00	1.00	1.00	1.00
	Gaussian width (eV)	—	1.10	1.10	1.10	1.10

Table 4. Voigt fitting parameters of the Ga 3d doublet on the Ga–Ce–O sample. Spin–orbit splitting was set to 0.44 eV and the branching ratio to 0.69.

	Pd thickness (nm)	0.00	0.08	0.16	0.24	0.32
First oxide component	Binding energy $3d_{5/2}$ (eV)	20.50	20.06	19.90	19.88	19.86
	Relative intensity	0.61	0.62	0.61	0.61	0.60
	Lorentzian width (eV)	0.40	0.40	0.40	0.40	0.40
	Gaussian width (eV)	0.95	0.95	0.95	0.95	0.95
Second oxide component	Binding energy $3d_{5/2}$ (eV)	19.78	19.00	18.82	18.76	18.74
	Relative intensity	0.39	0.38	0.33	0.28	0.26
	Lorentzian width (eV)	0.86	0.20	0.20	0.20	0.20
	Gaussian width (eV)	0.85	0.85	0.85	0.85	0.85
Intermetallic component	Binding energy $3d_{5/2}$ (eV)	—	—	18.44	18.36	18.32
	Relative intensity	0.00	0.00	0.06	0.11	0.14
	Lorentzian width (eV)	—	—	0.12	0.12	0.12
	Gaussian width (eV)	—	—	0.31	0.31	0.31

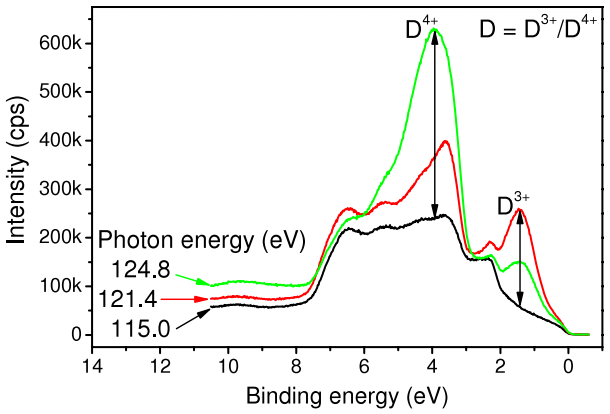

Figure 4. XPS valence band spectra measured on the prepared CeO_2 layer after the deposition of 0.32 nm of Pd at photon energy 115 eV (off-resonance), 121.4 eV (Ce^{3+} resonance around the binding energy 1.5 eV) and 124.8 eV (Ce^{4+} resonance around the binding energy 4 eV).

direct gallium–palladium bonds should play an important role also in the Pd/Ga–Ce–O system. Most probably Pd does not form small islands, like on less-interacting metal oxides, but an intermetallic phase with gallium. To verify this hypothesis, Pd and Ga core levels were analysed.

Pd 3d spectra (not shown) exhibited shapes similar to the previous case (section 3.1) but the FWHMs were slightly lower and the binding energies were higher, similar to their behaviour in other Pd intermetallic systems, see [21] and references therein. The evolution of the Pd $3d_{5/2}$ binding energy is plotted in figure 1(b) by red squares. The binding energy shift is in the same direction as that caused by reduced screening effects on very small particles, but in this case the quantitative extent, i.e. the size of the shift, is much larger than on the Pd/CeO_2 system described in section 3.1 (black stars in figure 1(b)). We believe that the shift of the binding energy with increasing thickness of palladium is caused by a change of the stoichiometry of the Ga–Pd intermetallic alloy.

Ga $2p_{3/2}$ and Ga 3d spectra after each deposition step are plotted in figures 5(a) and (b), respectively. After the deposition of 0.08 nm of Pd the Ga $2p_{3/2}$ peak assigned to oxidized gallium atoms in Ga–Ce–O shifted by about 0.5 eV towards lower binding energy and remained at this energy with further deposition steps. A similar shift appeared in the Ga 3d spectra, but in this case it was followed by a change of the intensity ratio between both fitted components and continued slightly (by 0.2 eV more) after the second deposition (0.16 nm of Pd). A more important result is the appearance of new narrower features in both Ga $2p_{3/2}$ and 3d spectra. They are assigned to metallic gallium or intermetallic gallium–palladium states and their intensity increases after each deposition of Pd. It seems that the Ga–Pd interaction breaks the bond between gallium and cerium oxide and two phases occur—the Ga–Ce–O mixed oxide with lower Ga content and the Ga–Pd alloy. It explains why the relative contribution of the Ce^{3+} states with respect to the Ce^{4+} ones mapped by the Ce 3d spectra and resonance enhancements in the valence band decreases. The reason for the saturation-like behaviour (i.e. that the dependence becomes less and less steep) of both Ce^{3+}/Ce^{4+} and D ratios is most probably that a stable Ga–Pd stoichiometry is reached.

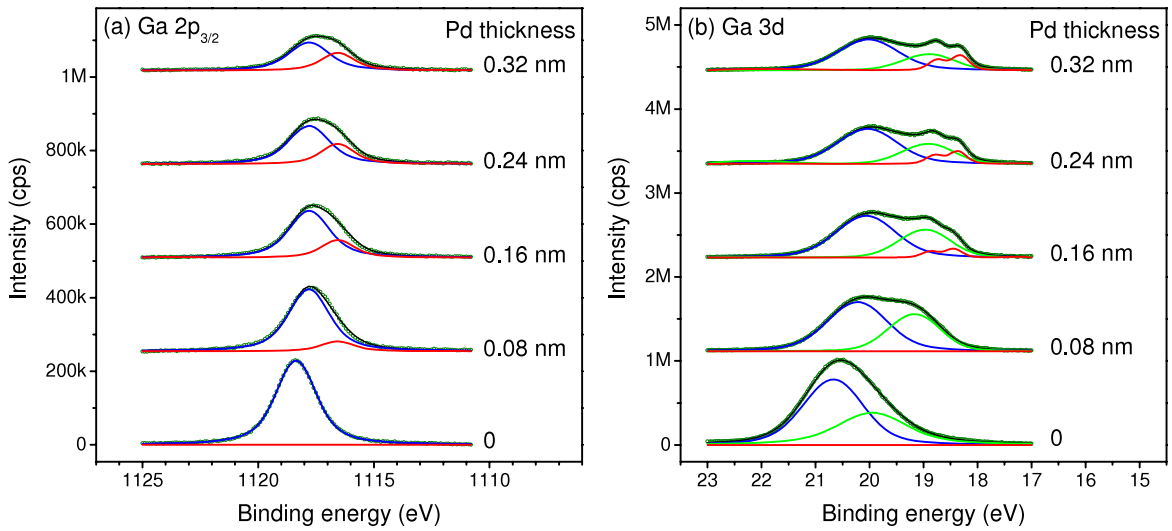

Figure 5. XPS spectra of Ga $2p_{3/2}$ (photon energy 1486.6 eV) (a) and Ga 3d (photon energy 115 eV) (b) measured on the prepared Ga–Ce–O layer and after each deposition step of Pd. The fits of the spectra with oxide and intermetallic components is shown.

Table 5. Voigt fitting parameters of the Ce 3d levels on the Pd/Sn–Ce–O sample with 0.07 nm of Sn. The spin–orbit splitting, asymmetry modelling, widths and branching ratios are the same as in table 1.

	Pd thickness (nm)	0.00	0.08	0.16	0.24	0.32
Ce^{4+}	Binding energy $3d_{5/2}$ (eV)	882.45	882.40	882.40	882.40	882.40
$u + v$	Relative intensity	0.27	0.29	0.29	0.29	0.28
Ce^{4+}	Binding energy $3d_{5/2}$ (eV)	889.00	888.95	888.95	888.95	888.95
$u'' + v''$	Relative intensity	0.32	0.35	0.35	0.35	0.34
Ce^{4+}	Binding energy $3d_{5/2}$ (eV)	898.45	898.40	898.40	898.40	898.40
$u''' + v'''$	Relative intensity	0.29	0.31	0.31	0.31	0.31
Ce^{3+}	Binding energy $3d_{5/2}$ (eV)	880.70	880.65	880.65	880.65	880.65
$u_0 + v_0$	Relative intensity	0.02	0.01	0.01	0.01	0.01
Ce^{3+}	Binding energy $3d_{5/2}$ (eV)	885.30	885.25	885.25	885.25	885.25
$u' + v'$	Relative intensity	0.10	0.04	0.04	0.04	0.06

3.3. Pd/Sn–Ce–O system

The interaction of tin with CeO_2 layers at 520 K was studied in the past [15, 16], and recently we compared those results with similar experiments performed at 120 and 300 K [19]. At 300 K two different tin thicknesses were studied—0.07 and 0.67 nm. Similar to the gallium case, tin–cerium mixed oxides of different stoichiometry were established. Ce^{3+} states appeared in the Ce 3d spectra and the Ce^{3+}/Ce^{4+} ratio was 0.14 and 0.52, respectively, see the fitting details in tables 5 and 6. The values of the D ratio obtained by the evaluation of the resonance enhancements of the valence band states were 0.9 and 2.3, respectively. In the present paper we describe the deposition of palladium at 300 K onto the Sn–Ce–O layers prepared in the same way. The choice of these two coverages of tin in the Sn–Ce–O layer was that, after the deposition of an 0.07 nm thick layer of Sn onto the CeO_2 surface, all tin atoms were oxidized and no features belonging to metallic tin appeared in the spectra (see the bottom curves in figures 6(a) and (b)). At higher tin coverage (0.67 nm), the spectra exhibited two different oxidation states, see figures 6(c) and (d)—broader features at higher binding energies attributed to oxidized tin atoms in the Sn–Ce–O layer and narrower peaks at lower binding energies representing excessive metallic tin on the sample surface that did not diffuse inside the ceria layer and oxidize. The parameters of the fitting are in tables 7, 8, 9 and 10.

For the analysis of the Sn 3d spectra we used the $3d_{3/2}$ peak instead of the usual $3d_{5/2}$ one to avoid the influence of the x-ray satellites of the $3d_{3/2}$ line overlapping the $3d_{5/2}$ one on the evaluation. For comparison with the literature dealing with the $3d_{5/2}$ line the reader should subtract the value of the spin–orbit splitting (8.41 eV [22]) from the binding energy of the $3d_{3/2}$ line presented here.

Similar to the gallium case, the oxide contribution to the Sn spectra slightly shifted after the first deposition step of palladium (0.08 nm) towards lower binding energy and kept this position after the following steps. On the sample with 0.07 nm of tin (figures 6(a) and (b)) the presence of palladium causes the appearance of an (inter)metallic feature at lower binding energy that was not present before. This feature can be attributed either to metallic tin or to Pd–Sn intermetallic alloy since the binding energies of Sn in both systems are very similar [21, 23] and do not depend strongly on the alloy stoichiometry. However, the formation of the Pd–Sn alloy is

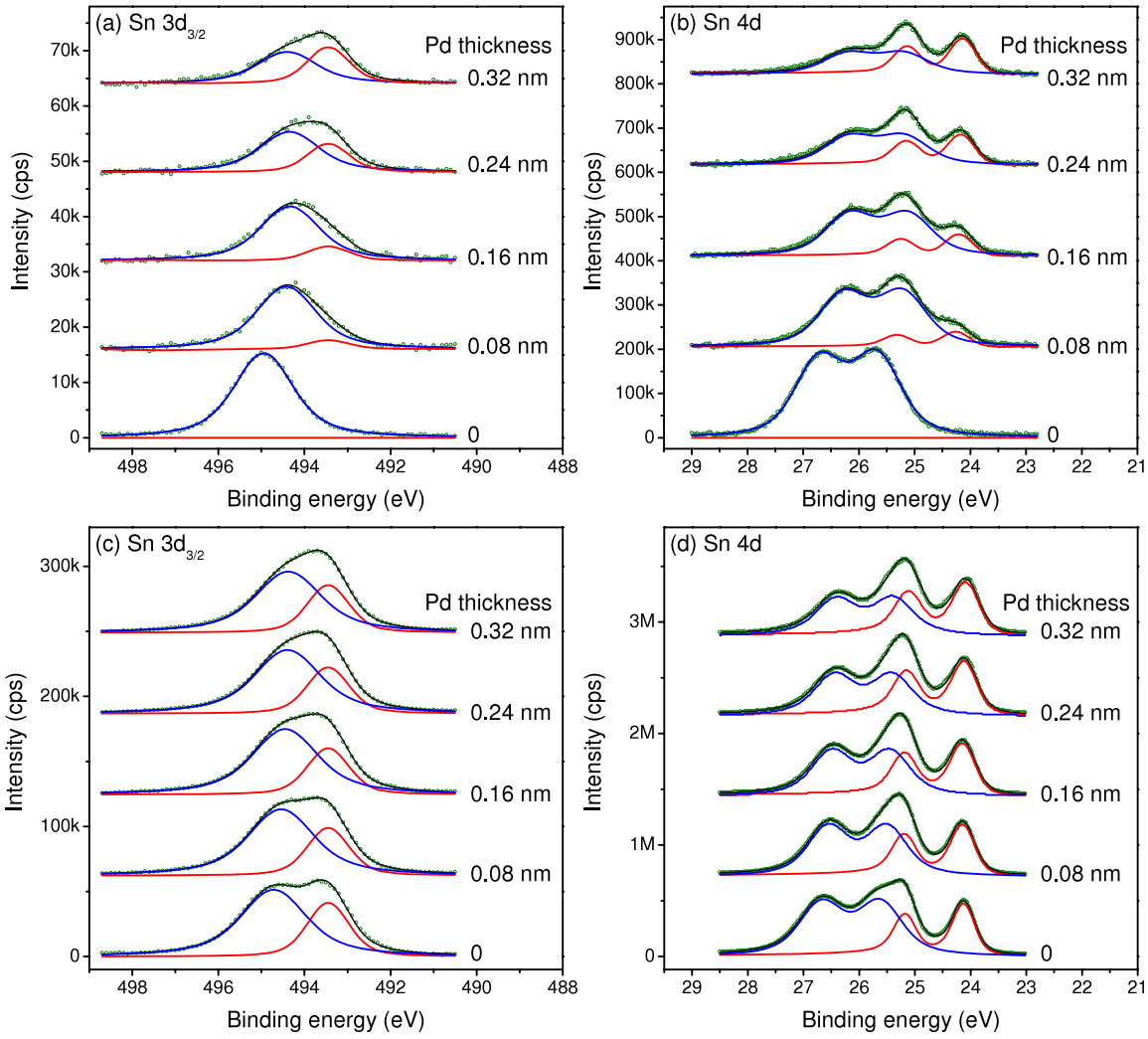

Figure 6. XPS spectra of Sn $3d_{3/2}$ (photon energy 1486.6 eV) ((a), (c)) and Sn 4d (photon energy 115 eV) ((b), (d)) measured on the Sn–Ce–O layers prepared by the deposition on 0.07 nm ((a), (b)) and 0.67 nm ((c), (d)) of Sn onto the CeO_2 layer. Fits of the spectra after each deposition step of Pd with oxide and (inter)metallic components is shown.

Table 6. Voigt fitting parameters of the Ce 3d levels on the Pd/Sn–Ce–O sample with 0.67 nm of Sn. The spin–orbit splitting, asymmetry modelling, widths and branching ratios are the same as in table 1.

	Pd thickness (nm)	0.00	0.08	0.16	0.24	0.32
Ce^{4+}	Binding energy $3d_{5/2}$ (eV)	882.55	882.55	882.50	882.50	882.50
$u + v$	Relative intensity	0.22	0.22	0.23	0.23	0.23
Ce^{4+}	Binding energy $3d_{5/2}$ (eV)	889.10	889.10	889.05	889.05	889.05
$u'' + v''$	Relative intensity	0.21	0.21	0.22	0.23	0.23
Ce^{4+}	Binding energy $3d_{5/2}$ (eV)	898.50	898.50	898.50	898.50	898.50
$u''' + v'''$	Relative intensity	0.23	0.23	0.24	0.24	0.25
Ce^{3+}	Binding energy $3d_{5/2}$ (eV)	880.75	880.75	880.75	880.75	880.75
$u_0 + v_0$	Relative intensity	0.07	0.07	0.06	0.06	0.06
Ce^{3+}	Binding energy $3d_{5/2}$ (eV)	885.35	885.35	885.35	885.35	885.35
$u' + v'$	Relative intensity	0.27	0.27	0.25	0.24	0.23

much more probable. Firstly, it is not likely that palladium would reduce tin without forming any intermetallic compound because, in such a case, to break tin–ceria bonds would require a strong interaction between palladium and ceria. It was shown in section 3.1 that this interaction is much weaker than that between tin and ceria. A second reason why we favour the formation of the intermetallic compound is the binding energy of the Pd $3d_{5/2}$ peak, figure 1(b). Its value decreases slowly from 335.7 to 335.45 eV with increasing amount of palladium, i.e. it remains again higher than that of clean

Table 7. Voigt fitting parameters of the Sn $3d_{3/2}$ line on the Sn–Ce–O sample with 0.07 nm of Sn.

	Pd thickness (nm)	0.00	0.08	0.16	0.24	0.32
Oxide component	Binding energy (eV)	494.95	494.40	494.35	494.35	494.40
	Relative intensity	1.00	0.92	0.86	0.69	0.57
	Lorentzian width (eV)	0.95	0.95	0.95	0.95	0.95
	Gaussian width (eV)	1.05	1.05	1.05	1.05	1.05
Intermetallic component	Binding energy (eV)	—	493.45	493.45	493.45	493.45
	Relative intensity	0.00	0.08	0.14	0.31	0.43
	Lorentzian width (eV)	—	0.43	0.43	0.43	0.43
	Gaussian width (eV)	—	0.90	0.90	0.90	0.90

Table 8. Voigt fitting parameters of the Sn $3d_{3/2}$ line on the Sn–Ce–O sample with 0.67 nm of Sn.

	Pd thickness (nm)	0.00	0.08	0.16	0.24	0.32
Oxide component	Binding energy (eV)	494.70	494.55	494.45	494.40	494.35
	Relative intensity	0.69	0.71	0.72	0.71	0.70
	Lorentzian width (eV)	1.20	1.20	1.20	1.20	1.20
	Gaussian width (eV)	1.05	1.05	1.05	1.05	1.05
(Inter)metallic component	Binding energy (eV)	493.45	493.45	493.45	493.45	493.45
	Relative intensity	0.31	0.29	0.28	0.29	0.30
	Lorentzian width (eV)	0.43	0.43	0.43	0.43	0.43
	Gaussian width (eV)	0.90	0.90	0.90	0.90	0.90

Table 9. Fitting parameters of the Sn 4d doublet on the Sn–Ce–O sample with 0.07 nm of Sn. The oxide component was fitted by a Voigt doublet with the spin–orbit splitting set to 1.04 eV and the branching ratio to 0.99. The intermetallic component was fitted by a convolution of the Doniach-Šunjić doublet with a Gaussian, the spin–orbit splitting was set to 1.04 eV, the asymmetry parameter to 0.09 and the branching ratio to 0.75.

	Pd thickness (nm)	0.00	0.08	0.16	0.24	0.32
Oxide component	Binding energy $4d_{5/2}$ (eV)	25.68	25.22	25.12	25.20	25.20
	Relative intensity	1.00	0.88	0.81	0.66	0.57
	Lorentzian width (eV)	0.50	0.50	0.50	0.50	0.50
	Gaussian width (eV)	0.73	0.73	0.73	0.73	0.73
Intermetallic component	Binding energy $4d_{5/2}$ (eV)	—	24.24	24.18	24.14	24.12
	Relative intensity	0.00	0.12	0.19	0.34	0.43
	Lorentzian width (eV)	—	0.04	0.04	0.04	0.04
	Gaussian width (eV)	—	0.53	0.53	0.53	0.53

Table 10. Fitting parameters of the Sn 4d doublet on the Sn–Ce–O sample with 0.67 nm of Sn. The peak shapes and common parameters for both components are the same as in table 9.

	Pd thickness (nm)	0.00	0.08	0.16	0.24	0.32
Oxide component	Binding energy $4d_{5/2}$ (eV)	25.62	25.50	25.44	25.40	25.38
	Relative intensity	0.69	0.64	0.61	0.57	0.55
	Lorentzian width (eV)	0.59	0.59	0.59	0.59	0.59
	Gaussian width (eV)	0.51	0.51	0.51	0.51	0.51
(Inter)metallic component	Binding energy $4d_{5/2}$ (eV)	24.11	24.12	24.12	24.10	24.06
	Relative intensity	0.31	0.36	0.39	0.43	0.45
	Lorentzian width (eV)	0.21	0.21	0.21	0.21	0.21
	Gaussian width (eV)	0.39	0.39	0.39	0.39	0.39

palladium. Most probably the stoichiometry of the Pd–Sn alloy is changing. On the Sn–Ce–O layer with 0.67 nm of tin, the components at lower binding energies in the Sn $3d_{3/2}$ and Sn 4d spectra (red curves in figures 6(c) and (d)) represent both metallic tin and Pd–Sn alloy features that are overlapping each other. In the more sensitive Sn 4d spectra one can clearly see that with increasing coverage of palladium the (inter)metallic component becomes stronger with respect to the Sn–Ce–O-related one.

In figure 3 the evolution of the Ce^{3+}/Ce^{4+} and of the D ratio is plotted. Upon palladium deposition onto the Sn–Ce–O surface with 0.67 nm of tin, there is a slow decrease with increasing Pd thickness, i.e. the same trend as observed in the Ga–Ce–O case described in section 3.2. This decrease

is less steep, which is most probably caused by an excess of tin in this surface layer (contrary to the gallium case, the amount of tin is so high that there is not only the oxidized but also the metallic, phase present). Also the binding energy of the Pd $3d_{5/2}$ peak (figure 1(b)) lying above 336 eV for all deposition steps of palladium in comparison to the data in [21] suggest an excess of Sn in the Pd–Sn alloy. On the sample of Pd deposited onto a Sn–Ce–O layer with a lower amount of tin (0.07 nm) we expected to see better the effects of the Pd–Sn interaction and the results are very surprising. Upon the deposition of palladium, both the Ce^{3+}/Ce^{4+} and the *D* ratios (green circles) at first slowly decreased, i.e. the trend was in the same direction as in the Ga–Ce–O and 0.67 nm Sn–Ce–O cases, then reached a local minimum around the palladium thickness 0.2 nm and it started to increase very slowly again. We believe that in our experiments the shape of the Ce^{3+}/Ce^{4+} and of the *D* ratios' evolution are combining two opposite trends: (i) palladium strongly interacts with Ga and Sn and causes breaking of the bonds between these two metals and ceria that can reoxidize back to the original Ce^{4+} state and (ii) Pd itself interacts with the ceria layer and induces its partial reduction and a creation of oxygen vacancies in the Ce^{4+} structure (section 3.1). At the minimum point of the discussed dependences plotted by green circles in figure 3 the binding energy of the Pd $3d_{5/2}$ peak is 335.5 eV which, according to [21], corresponds to a stoichiometry of Pd_3Sn, i.e. the most stable Pd–Sn alloy stoichiometry according to the phase diagram [24].

4. Conclusions

The interaction of palladium with CeO_2 and two mixed oxides—Ga–Ce–O and Sn–Ce–O—was studied by photoelectron spectroscopy of the core levels and the valence band resonances in the Ce 4d $\rightarrow$ 4f photoabsorption region. It was confirmed that, on the stoichiometric ceria, Pd grows in the form of islands and interacts relatively weakly with the oxide support. Nevertheless, some Ce^{3+} states appear on the ceria surface. In contrast to this, on both mixed oxides which have a high Ce^{3+} content, Pd interacts strongly with both added metals leading to formation of Pd–Ga(Sn) intermetallic bonds at the cost of the Ga(Sn)–Ce–O ones. In this case the contribution of Ce^{3+} states decreases and ceria reoxidizes back to the original Ce^{4+} oxidation state. This study is important for the design of catalysts for low-temperature CO oxidation where palladium provides adsorption sites for the molecules of CO while ceria, due to its oxygen storage capacity, acts as the source of oxygen atoms for the reaction.

Acknowledgments

The authors acknowledge the support of the Ministry of Education of the Czech Republic under grant nos. LC06058, LA08022 and MSM 0021620834.

References

[1] Xiao W, Guo Q and Wang E G 2003 *Chem. Phys. Lett.* **368** 527–31
[2] Nguyen T B, Deloume J P and Perrichon V 2003 *Appl. Catal.* A **249** 273–84
[3] Luo M-F, Hou Z-Y, Yuan X-X and Zheng X-M 1998 *Catal. Lett.* **50** 205–9
[4] Sennanayake S D, Zhou J, Baddorf A P and Mullins D R 2007 *Surf. Sci.* **601** 3215–23
[5] Craciun R, Daniell W and Knözinger H 2002 *Appl. Catal.* A **230** 153–68
[6] Pecchi G, Reyes P, López T and Gómez R 2004 *J. Non-Cryst. Solids* **345/346** 624–7
[7] Gopinath R, Lingaiah N, Sreedhar B, Suryanarayana I, Sai Prasad P S and Obuchi A 2003 *Appl. Catal.* B **46** 587–94
[8] Usami Y, Kagawa K, Kawazoe M, Matsumura Y, Sakurai H and Haruta M 1998 *Appl. Catal.* A **171** 123–30
[9] Idriss H 2004 *Platinum Met. Rev.* **48** 105–15
[10] Roy S and Hegde M S 2008 *Cat. Commun.* **9** 811–5
[11] Wilson E L, Chen Q, Brown W A and Thornton G 2007 *J. Phys. Chem.* C **111** 14215–22
[12] Yang Z, Lu Z, Luo G and Hermansson K 2007 *Phys. Lett.* A **369** 132–9
[13] Matsumoto M, Soda K, Ichikawa K, Tanaka S, Taguchi Y, Jouda K, Aita O, Tezuka Y and Shin S 1994 *Phys. Rev.* B **50** 11340–6
[14] Skála T, Šutara F, Cabala M, Škoda M, Prince K C and Matolín V 2008 *Appl. Surf. Sci.* **254** 6860–4
[15] Matolín V, Cabala M, Cháb V, Matolínová I, Prince K C, Škoda M, Skála T and Veltruská K 2008 *Surf. Interface Anal.* **40** 225–30
[16] Škoda M, Cabala M, Cháb V, Prince K C, Sedláček L, Skála T, Šutara F and Matolín V 2008 *Appl. Surf. Sci.* **254** 4375–9
[17] Šutara F, Cabala M, Cháb V, Prince K C, Sedláček L, Skála T, Škoda M and Matolín V 2008 *Thin Solid Films* **516** 6120–4
[18] Tsud N, Johánek V, Stará I, Veltruská K and Matolín V 2000 *Surf. Sci.* **467** 169–76
[19] Skála T, Šutara F, Prince K C and Matolín V 2008 *J. Electron Spectrosc. Relat. Phenom.* at press doi:10.1016/j.elspec.2008.10.003
[20] Skála T, Bača D, Libra J, Tsud N, Nehasil V, Nemšák S, Prince K C and Matolín V 2008 *Thin Solid Films* **517** 773–8
[21] Skála T, Veltruská K, Sedláček L, Mašek K, Matolínová I and Matolín V 2007 *Appl. Surf. Sci.* **253** 5400–3
[22] Chastain J (ed) 1992 *Handbook of X-ray Photoelectron Spectroscopy* (Eden Prairie, MN: Perkin-Elmer)
[23] Tsud N, Skála T, Šutara F, Veltruská K, Dudr V, Fabík S, Sedláček L, Cháb V, Prince K C and Matolín V 2005 *Surf. Sci.* **595** 138–50
[24] Massalski T B 1990 *Binary Alloy Phase Diagrams* 2nd edn, vol 3 (Metals Park, OH: ASM) p 3049